Prion induction involves an ancient system for the sequestration of aggregated proteins and heritable changes in prion fragmentation

Jens Tyedmers[a,b], Sebastian Treusch[a,c], Jijun Dong[a], J. Michael McCaffery[d], Brooke Bevis[a,c], and Susan Lindquist[a,c,1]

[a]Whitehead Institute for Biomedical Research, Cambridge, MA 02142; [b]Zentrum fuer Molekulare Biologie Heidelberg, DKFZ-ZMBH-Alliance, Universitaet Heidelberg, D-69120 Heidelberg, Germany; [c]Howard Hughes Medical Institute, Department of Biology, Massachusetts Institute of Technology, Cambridge, MA 02139; and [d]Integrated Imaging Center and Department of Biology, The Johns Hopkins University, Baltimore, MD 21218

Contributed by Susan Lindquist, March 29, 2010 (sent for review December 16, 2009)

When the translation termination factor Sup35 adopts the prion state, [*PSI*$^+$], the read-through of stop codons increases, uncovering hidden genetic variation and giving rise to new, often beneficial, phenotypes. Evidence suggests that prion induction involves a process of maturation, but this has never been studied in detail. To do so, we used a visually tractable prion model consisting of the Sup35 prion domain fused to GFP (PrD-GFP) and overexpressed it to achieve induction in many cells simultaneously. PrD-GFP first assembled into Rings as previously described. Rings propagated for many generations before the protein transitioned into a Dot structure. Dots transmitted the [*PSI*$^+$] phenotype through mating and meiosis, but Rings did not. Surprisingly, the underlying amyloid conformation of PrD-GFP was identical in Rings and Dots. However, by electron microscopy, Rings consisted of very long uninterrupted bundles of fibers, whereas Dot fibers were highly fragmented. Both forms were deposited at the IPOD, a biologically ancient compartment for the deposition of irreversibly aggregated proteins that we propose is the site of de novo prion induction. We find that oxidatively damaged proteins are also localized there, helping to explain how proteotoxic stresses increase the rate of prion induction. Curing PrD-GFP prions, by inhibiting Hsp104's fragmentation activity, reversed the induction process: Dot cells produced Rings before PrD-GFP reverted to the soluble state. Thus, formation of the genetically transmissible prion state is a two-step process that involves an ancient system for the asymmetric inheritance of damaged proteins and heritable changes in the extent of prion fragmentation.

yeast prion | fiber fragmentation | IPOD (Insoluble Protein Deposit) | prion inheritance | asymmetric damage distribution

Prions are self-perpetuating protein conformations that store and transmit phenotypic information independently of nucleic acids. In fungi, they act as protein-based elements of heredity, stably propagating their altered protein conformations and associated phenotypes (1, 2).

In *Saccharomyces cerevisiae*, seven prions are known (3) and evidence indicates that numerous other yeast proteins are capable of forming prions (4). The proteins have different molecular functions and produce different prion phenotypes. Although they share no sequence homology, their prion domains (PrDs) are enriched in asparagine and glutamine residues. These PrDs can adopt self-perpetuating prion conformations that are amyloids. They template the conversion of soluble prion proteins of the same type to the same conformation (1, 2). The AAA+ ATPase Hsp104 shears amyloid fibers to generate prion seeds, also referred to as propagons (5), facilitating inheritance of the prion state from generation to generation (6).

The protein determinant for the prion [*PSI*$^+$] is the translation termination factor Sup35. Sup35's PrD, NM, has an N-terminal amyloidogenic domain (N) and a solubilizing middle domain (M) (1, 2). In vitro, purified PrD can form amyloid fibrils on its own (7). In vivo, assembly of the prion reduces the availability of soluble, functional termination factor. This causes stop codon read-through (1, 2) and results in a large array of diverse phenotypes depending on the genetic background (8). Stressful conditions alter protein folding homeostasis and increase the rate at which cells switch to the prion state, creating a bet-hedging strategy for survival in fluctuating environments (3, 4, 9).

[*PSI*$^+$] propagation is well studied. However, the spontaneous de novo formation of [*PSI*$^+$] is rare and poorly understood. Overexpression of Sup35, or its PrD, dramatically increases the frequency of [*PSI*$^+$] induction (10), offering an opportunity to investigate the process. During prion induction, two distinct aggregation patterns are observed: ribbon and ring structures that extend throughout the cell and round dot structures (11, 12). Dots correspond to the mature [*PSI*$^+$] prion state. The ring structures appear to be a hallmark of de novo [*PSI*$^+$] induction, but their nature remains a mystery. This is the subject of our investigation.

Results

Expression of PrD-GFP in a Sup35 PrD Deletion Strain Results in Rings and Dots. To study the de novo formation and inheritance of prion amyloid in vivo on a single-cell level, we employed a fusion of the PrD (NM) with GFP, which is soluble in [*prion*$^-$] cells but faithfully propagates with the wild-type Sup35 amyloid in [*PRION*$^+$] cells (13). To determine whether this visually tractable protein is fully capable of forming a prion in its own right, we expressed it from the Sup35 promoter to maintain normal expression. When these cells were mated to [*psi*$^-$] cells, the protein remained soluble. When mated to [*PSI*$^+$] cells, it acquired the prion state (Fig. S1), was dominant in matings, and segregated 4:0 in meiosis. Thus, PrD-GFP fully recapitulates prion behavior. However, as expected, spontaneous switches to the prion state were too rare to be observed.

To provide a robust system for studying prion induction, we placed the PrD-GFP fusion under the control of the GPD promoter, which increased its expression ~15-fold, and integrated a single copy into the genome, to keep expression uniform in each cell. We also deleted the PrD from the endogenous *SUP35* gene, making the translation termination domain immune from sequestration into the prion, which can be toxic when it happens excessively (10, 14).

Soon after transformation, while cells were still in microcolonies, they had the diffuse GFP-fluorescence of [*prion*$^-$] cells. In more mature colonies, a large fraction of cells displayed

Author contributions: J.T., S.T., J.D., J.M.M., B.B., and S.L. designed research; J.T., J.D., J.M.M., and B.B. performed research; J.T., J.D., J.M.M., B.B., and S.L. analyzed data; and J.T., S.T., and S.L. wrote the paper.

The authors declare no conflict of interest.

[1]To whom correspondence should be addressed. E-mail: lindquist_admin@wi.mit.edu.

This article contains supporting information online at www.pnas.org/lookup/suppl/doi:10.1073/pnas.1003895107/-/DCSupplemental.

CELL BIOLOGY

a large ring-, rod-, or ribbon-like structure of PrD-GFP fluorescence (collectively referred to as "Rings" throughout this article). This Ring pattern was inherited for many generations. After two to eight restreaks, each representing ~25 generations, the aggregation pattern changed and PrD-GFP was exclusively found in one large focus per cell, hereafter referred to as Dots (Fig. 1*A*). Rings and Dots were previously described during prion induction in cells transiently overexpressing PrD-GFP in the presence of wild-type Sup35 (11, 12).

Propagation of Rings and Dots Is Independent of [*RNQ*$^+$]. When PrD-GFP was overexpressed in cells carrying a deletion of *RNQ1*, a factor required for efficient prion induction (15–17), it remained diffuse (11) (Fig. S2). When cells containing Rings or Dots were mated to cells with a *RNQ* deletion and sporulated, haploid progeny with the deletion maintained their Rings and Dots (Fig. S3). Thus, as for the [*PSI*$^+$] prion itself (18), Dots and Rings require [*RNQ*$^+$] for their induction but not their propagation.

Time-Lapse Microscopy Establishes Stable Asymmetric Inheritance of Both Aggregation States. We followed the propagation of PrD-GFP Rings and Dots for several cell divisions using time-lapse microscopy (Fig. 1*B*). Both were faithfully propagated, but Rings were less stable, frequently giving rise to progeny with diffuse fluorescence (Fig. 1*B Upper*, cells encircled by dotted line). Surprisingly, during cell division, Rings and Dots were retained in mother cells. Visible assemblies only became detectable in daughter cells after the dividing septum had formed. Cells with Rings initially gave rise to daughters with a single small focus, much like the initiating focus in Dot cells, but these generally expanded to form a typical Ring structure by the time the cell was ready for a new division (Fig. 1*B Upper*).

PrD-GFP Dots Can Transmit the [*PSI*$^+$] Phenotype but Rings Cannot. Genetically, a defining feature of prions is dominance in crosses to mating partners. We first mated Ring and Dot cells to isogenic partners whose *RNQ1* gene had been deleted before PrD-GFP expression. As noted above, this kept their PrD-GFP protein in the diffuse nonprion state. After mating, diffuse PrD-GFP converted to the Ring or Dot form of its mating partner. When these diploids were sporulated, all haploid progeny of Dot matings contained Dots. Rings were also inherited, albeit less faithfully (Fig. S3).

Next, we mated Ring and Dot cells to wild-type [*psi*$^-$] cells to determine whether they could transmit the [*PSI*$^+$] phenotype. Both Rings and Dots were maintained in the diploids. All cells carried the *ade1-14* stop codon mutation (1), but because one Sup35 allele carried a PrD deletion, the [*PSI*$^+$] read-through phenotype could not be detected in the diploid. However, after sporulation, haploid progeny that received the wild-type *SUP35* gene and whose protein had acquired the [*PSI*$^+$] state switched colony color from red to pink (Fig. 2*A*).

In control matings, parents with diffuse PrD-GFP fluorescence produced only red [*psi*$^-$] progeny (Fig. 2*A Top*). Progeny of Dot parents that received only the wild-type Sup35 gene invariably gave rise to pink [*PSI*$^+$] colonies as expected of faithful transmission of the prion state from PrD-GFP to wild-type Sup35 (Fig. 2*A Bottom*). Also, progeny carrying both wild-type Sup35 and the PrD-GFP overexpression construct were never recovered, because of excessive, toxic sequestration of Sup35 (10, 14). Surprisingly, mating with Ring cells produced no wild-type Sup35 progeny with the [*PSI*$^+$] phenotype (Fig. 2*A Middle*). Furthermore, cells carrying both the PrD-GFP construct and wild-type Sup 35 were readily obtained (e.g., Fig. 2*A Middle*, spore III). In these cells, PrD-GFP maintained its initial Ring pattern, demonstrating that Rings generally propagated faithfully during meiosis.

A simple explanation might be that the PrD-GFP in Ring cells does not interact with WT Sup35. To test this, we induced PrD-GFP Rings and Dots in cells with HA-tagged Sup35 protein as

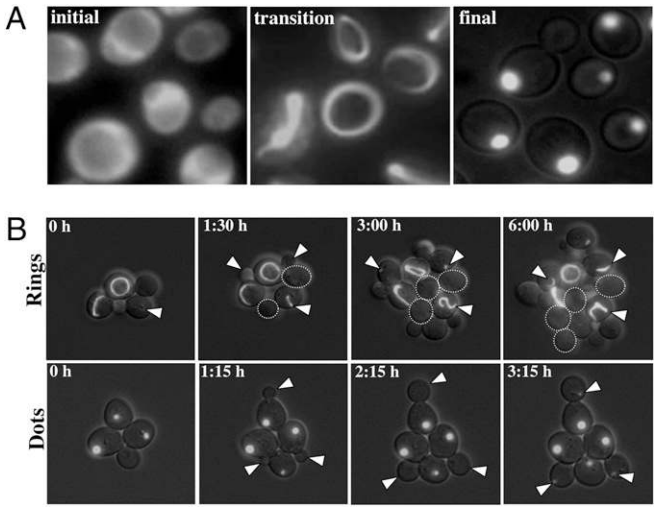

Fig. 1. Expression of PrD-GFP at high levels produces self-propagating Ring assemblies that transition to a Dot assembly only after many generations. (*A*) Cells constitutively expressing PrD-GFP under control of the GPD promoter are shown at different times. Initial, immediately after transformation of the expression construct; transition, transformants after 3–5 days; final, transformants after ~10 days (hundreds of generations). (*B*) Haploid cells propagating either PrD-GFP Rings (*Upper*) or Dots (*Lower*). Cell divisions (arrows) were followed microscopically. Images represent a merge of several focal planes of GFP fluorescence overlaid with single DIC focal plane. A dotted line encircles progeny of Ring mothers that did not form any aggregates during the course of the experiment.

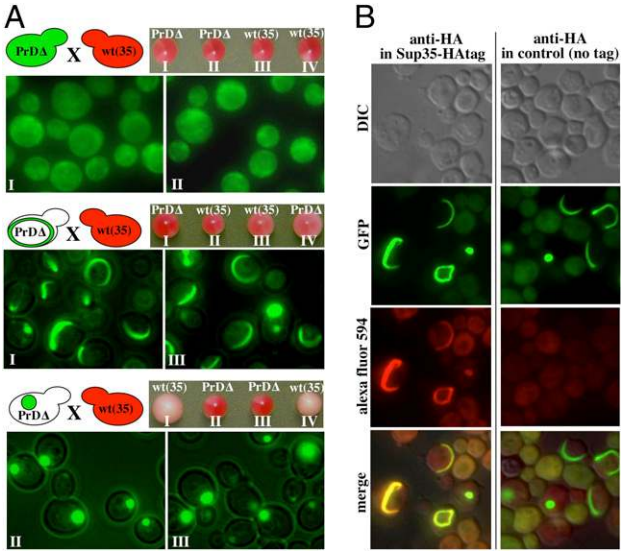

Fig. 2. Cells with Rings do not induce the [*PSI*$^+$] prion state in a mating partner. (*A*) Haploid strains carrying a PrD deletion of the endogenous SUP35 gene (PrDΔ) displaying diffuse PrD-GFP fluorescence, Rings or Dots were mated with a wild-type SUP35 [*psi*$^-$] strain. The resulting diploids were sporulated and tetrads were dissected. Spores with the PrD-GFP fusion were analyzed by fluorescence microscopy. Colony colors of the progeny ([*psi*$^-$], red; [*PSI*$^+$], light pink) revealed that Dots, but not Rings, induced the prion state of wild-type SUP35. (*B*) Sup35-HA colocalizes with PrD-GFP Rings and Dots. A [*psi*$^-$] strain carrying an inducible copy of PrD-GFP and a C-terminally HA-tagged Sup35 (SUP35-HA) was analyzed by immunofluorescence and fluorescence microscopy. Colocalization is shown in yellow in merged images.

the only source of this essential protein. HA colocalized with both Rings and Dots (Fig. 2*B*), eliminating this possibility.

In Ring and Dot Cells, PrD-GFP Is in the Same Amyloid Conformation. A common feature of prions is the ability to exist in several related, but distinct, amyloid conformations, known as "prion strains" (19, 20). These propagate with different polymerization and fragmentation efficiencies. Because they reach different equilibria between the soluble functional form and the amyloid, they produce distinct phenotypes (in *ade1-14* cells, colonies with different shades of pink) (19–21). Thus, another explanation for our results might be that Rings represent a different prion strain than Dots, one that is too "weak" to elicit a detectable phenotype. This occurs, for example, with the [ETA^+] variant of [PSI^+] (22).

When crude cell lysates of all cell types were boiled in SDS, they all produced a PrD-GFP band of the same intensity by SDS/PAGE, confirming that the protein was expressed at the same level (Fig. 3*A Upper*). When analyzed without boiling on semidenaturing agarose gels, the PrD-GFP protein of both Ring and Dot cells migrated as high-molecular-weight SDS-resistant complexes typical of prion amyloids (Fig. 3*A Lower Left*).

Next, we tested the ability of Dots and Rings to seed polymerization of purified soluble PrD, a defining characteristic of prions. Lysates of cells with diffuse fluorescence did not seed polymerization, but lysates of Ring and Dot cells had very similar seeding capacities (Fig. 3*A Lower Right*): SDS-resistant species could be detected almost immediately, and their sizes increased similarly during the course of the experiment.

Proteins from different prion strains transform [psi^-] cells to [PSI^+] in a phenotype-specific manner. To minimize manipulations, crude extracts were introduced directly into [psi^-] cells to test for such differences (19, 20). To our surprise, lysates from cultures with Rings and Dots both gave rise to the same strong [PSI^+] strain (Fig. 3*B*): Dot lysates induced the strong prion phenotype in 71 transformants, the weak phenotype in only 3. Ring lysates induced the strong phenotype in 101 transformants, the weak in only 6.

Although the stability of amyloid structures makes it extremely unlikely that a weak conformation might convert to a strong one during our procedure (19, 20), we considered the possibility. We eliminated the sonication step before transformation and used several different lysis procedures without changing the outcome. More definitively, we performed many similar experiments with lysates from bona fide weak prion strains but never observed conversion of weak prion strains to strong. Thus, Rings and Dots do not represent different prion conformations or strains.

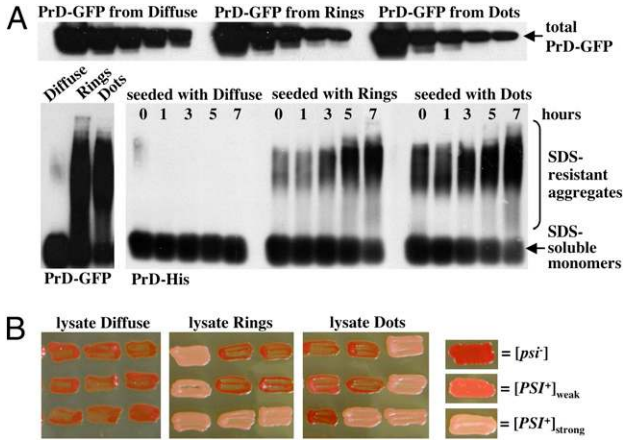

Fig. 3. Cells with Rings and Dots contain PrD-GFP in the same prion conformation. (*A Upper*) Crude lysates from cells displaying diffuse, Ring or Dot fluorescence were adjusted to equal protein concentrations and serial dilutions (1:2 steps) were loaded onto an SDS gel and analyzed by SDS/PAGE and Western blotting with an anti-GFP antibody to reveal the amounts of PrD-GFP in the different lysates. (*A Lower Left*) The three different lysates were analyzed by semidenaturing agarose gel analysis (SDD-AGE) followed by Western blotting with an anti-GFP antibody. Lysates from cells with Rings and Dots, but not diffuse PrD-GFP, contain SDS-resistant high-molecular-weight aggregates of PrD-GFP. (*A Lower Right*) Purified PrD-His was seeded with the three different lysates in vitro and analyzed by SDD-AGE and Western blotting with an anti-His-tag antibody. SDS-resistant high-molecular-weight aggregates were formed with comparable kinetics. (*B*) Protein transformations of a [psi^-] tester strain (red colony color) were performed with crude lysates from cells with diffuse PrD-GFP fluorescence or Rings and Dots. The prion status and strain of the transformants was determined by colony color. Both types of aggregates induced a strong [PSI^+] strain (light pink color) with similar efficiencies.

Aggregate Formation Occurs at a Site Specific to the Deposition of Insoluble Aggregates. We asked whether the differences in transmissibility of the [PSI^+] phenotype with Rings and Dots could be due to different cellular localizations. The vacuolar dye FM4-64 established that PrD-GFP Dots were localized adjacent to the vacuole (Fig. 4*A*, leftmost column). A single focus at the vacuole is characteristic of the pre-autophagosomal structure (PAS), which coordinates autophagosome formation and cytoplasm-to-vacuole vesicle trafficking (23). Colocalization of a PrD-YFP fusion and the CFP-tagged PAS markers ATG8 and ATG14 confirmed this localization (Fig. 4*A*). Dots were directly adjacent to the PAS. Rings intersected it (Fig. 4*A*).

Recently, a perivacuolar PAS-associated site for the deposition of irreversibly aggregated proteins was discovered and termed the IPOD for *I*nsoluble *PrO*tein *D*eposit (24). It also accumulates the Ure2 and Rnq1 proteins in their prion forms (24). To extend this characterization, we used mass spectrometry to identify proteins that were co-immunocaptured with PrD-GFP Dots but not with soluble PrD-GFP (Fig. S4). Rnq1 was among them (Table S1), confirming the capture of bona fide IPOD substrates. We also found proteins known to be very sensitive to oxidative damage (25).

CFP-tagged versions of Rnq1 and the two oxidation-sensitive proteins, Fas1 (fatty acid synthase) and Pdc1 (pyruvate decarboxylase 1) (25), were used to confirm cellular colocalization by microscopy. RNQ1-CFP colocalized with PrD-YFP Dots constitutively (Fig. 4*B*). The partial colocalization of Fas1 and Pdc1 with PrD-YFP Dots was most apparent after cells were treated with the oxidizing agent menadione (25) (Fig. 4*B*). Thus, the previously reported polarisome-dependent asymmetric inheritance of oxidatively damaged proteins (26, 27) occurs in part at the IPOD, which is also a site for prion accumulation.

Number of PrD-GFP Amyloid Fibers Differs Between Ring and Dot Aggregates. Next, we investigated the difference between Rings and Dots by transmission electron microscopy (TEM). We easily identified both forms by their highly ordered fibrous appearance, which closely resembled fibrils formed by Sup35 or PrD in vitro (7, 28). We confirmed that these assemblies were indeed PrD-GFP Rings and Dots by immuno-EM using an antibody against GFP (Fig. S5). We also found the typical electron-dense foci formed by amorphous aggregates of damaged proteins at this site (Fig. 5*A Lower* and Fig. S6), further confirming the colocalizations described above.

Rings and Dots were not separated from the surrounding cytoplasm by any compartmentalizing elements, such as membranes or cytoskeletal structures. Fibrils formed in vitro by the Sup35 PrD alone have an average diameter of ~11.5 nm, whereas fibrils of full-length Sup35 are ~25 nm (7, 28). In cross-sections, Ring and Dot PrD-GFP fibrils had identical doughnut-like morphologies with a diameter of ~25–30 nm and an inner core of 6–12 nm (Fig. S5). This is consistent with the prion domain forming the inner core of the fiber, surrounded by GFP molecules.

CELL BIOLOGY

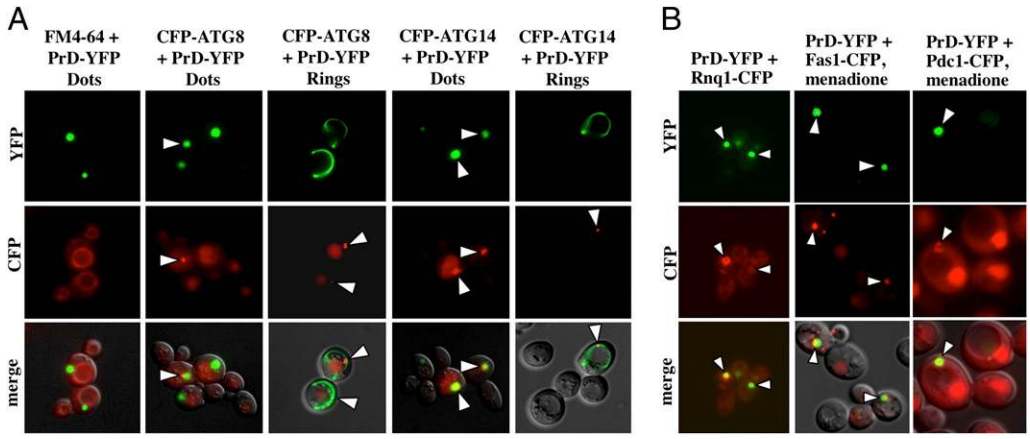

Fig. 4. Prion aggregates localize to the IPOD compartment as shown using markers for the pre-autophagosomal structure (PAS) and additional IPOD substrates. Cells carrying Dots were generated using a genomic copy of GPD-controlled PrD-YFP. Rings were induced using an analogous galactose-inducible construct. (*A*) FM4-64 visualization of the vacuolar membrane shows the perivacuolar localization of PrD-YFP Dots (leftmost column). The localization of Rings and Dots to the pre-autophagosomal structure was visualized using centromeric plasmids expressing N-terminal CFP fusions of ATG8 or ATG14. (*B*) Colocalization of PrD-YFP Dots with known and newly identified substrates of the IPOD compartment (indicated by arrows). Genomic copies of PDC1 or FAS1 were tagged with CFP (first and second columns), whereas the Rnq1-CFP fusion was expressed from a plasmid under control of the Cup1 promoter (third column). Aggregation of Pdc1-CFP or Fas1-CFP was induced using 0.1 or 2 mM menadione, respectively, for 4 h before microscopy. The Rnq1-CFP expression was induced using 100 μM copper sulfate. Images represent one single optical plane.

However, there was one profound difference between the fibrils in the Rings and Dots: their length. Rings contained bundles of very long uninterrupted fibrils (Fig. 5*A Upper*). Dots contained a profusion of short fibril bundles with diverse orientations in the same structure (Fig. 5*A Lower*). Thus, Ring and Dot aggregates displayed an extreme difference in fragmentation and, consequently, in the number of fibril ends. The cell lysis procedure used in our protein transformation or seeding assays (Fig. 3) would certainly fragment the very long fibrils of Ring cells, eliminating the sole difference between Rings and Dots.

In vivo, the only known protein with the capacity to sever PrD fibrils is the AAA+ ATPase Hsp104. Inhibition of Hsp104 increases the number of ring-bearing cells when PrD-GFP is overexpressed in the presence of wild-type Sup35 (11). However, the relationship between Hsp104 activity and Dots has never been examined. We inhibited Hsp104 activity in Dot cells by two different methods: incubation with 5 mM GdHCl, which selectively inhibits Hsp104's ATPase cycle (29) (Fig. 5*B*), and expression of a dominant negative mutant of Hsp104 (Fig. S7), which is incorporated into Hsp104 hexamers and blocks their activity. In both cases, time-lapse microscopy revealed that preexisting Dots never changed, but mother cells with Dots rapidly and invariably produced daughter cells with Rings. These Rings also remained intact. However, within just a few divisions, all Ring-containing cells gave rise to progeny with diffuse PrD-GFP fluorescence. Thus, the curing of Dots by Hsp104 inhibition mirrors their formation. The distinct states of prion maturation result from differences in the number of fiber fragments generated by Hsp104 and hence the number of prion seeds.

Discussion

We find that prion induction by the Sup35 PrD involves a maturation process with a distinct, stable, and heritable intermediate. Surprisingly, this intermediate (Ring state) has all of the biochemical characteristics of the mature prion (Dot state) but distinct phenotypic properties. It does not confer a [*PSI*$^+$] phenotype on meiotic progeny whose only source of Sup35 is the wild-type protein, even when PrD-GFP Rings coexist in the same cell. How might we resolve this seeming paradox and also decipher the nature of the prion induction process? Two other observations, we think, provide the key.

First, by electron microscopy, Ring fibrils are long and uninterrupted, and Dot fibrils are highly fragmented. Indeed, the degree of fiber fragmentation is the defining characteristic for the different structures, because blocking of Hsp104's fragmentation activity reverts Dots to Rings before the assemblies are lost entirely. Second, the deposition of Rings and Dots occurs at a site specific for the compartmentalization of damaged proteins, known as the IPOD (24). In cells undergoing mitosis, Rings and Dots are retained in mother cells but reform in their daughters at the IPOD immediately after septum formation. The most parsimonious explanation is that prion seeds, too small to be detected by fluorescence (30), are liberated by the activity of Hsp104 and transmitted to daughter cells.

Taking these observations together, we propose a model for prion induction (Fig. 6) that also explains the distinct phenotypes and heritable nature of Rings and Dots. Upon initial expression, PrD-GFP is soluble, but the intrinsically unstructured Sup35 PrD has a high propensity to misfold. This misfolded protein is targeted to the IPOD. Because nucleated conformational conversion to the prion state requires an oligomeric intermediate (31), the high local concentration of PrD-GFP at the IPOD increases the likelihood of prion induction (12). [*RNQ*$^+$] prions, which are required for [*PSI*$^+$] induction (15–17), are also located at the IPOD and ready to facilitate nucleation (this study and refs. 24 and 32).

Initially, only a few prion seeds form. Therefore, the rate at which soluble full-length Sup35 is sequestered from translation is limited. Rings formed in this way can coexist with the wild-type protein without causing toxicity or creating a [*PSI*$^+$] phenotype (Fig. 2*A Middle*, spore III). The small number of seeds creates long bundles of fibers, which appear as Rings confined only by the boundary of the cell. Inheritance of a small number of seeds by daughter cells perpetuates the Ring state.

Dots consist of short highly fragmented fibers. Increased fragmentation causes a larger number of prion seeds to be inherited by daughters, explaining the more stable inheritance of Dots relative to Rings and the ability to reliably transmit the prion state to all meiotic progeny. In this case, polymerization is limited by the amount of soluble prion protein and not by the number of prion seeds. Thus, meiotic progeny inheriting PrD-GFP Dots, whose only source of the essential Sup35 is the wild-type protein, are inviable.

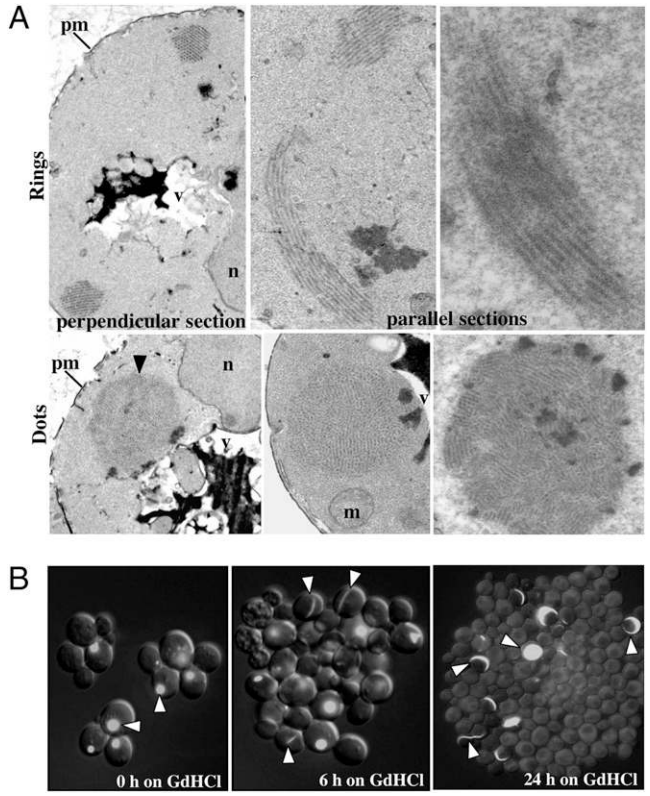

Fig. 5. Electron microscopy of Ring and Dot cells reveals the different degrees of PrD-GFP fibril fragmentation. (*A Upper*) Different magnifications of ultrathin cell section with a large Dot aggregate next to the vacuole. (*A Lower*) Perpendicular or parallel sections of a cell displaying PrD-GFP Rings. m, mitochondrion; n, nucleus; v, vacuole; pm, plasma membrane. (*B*) Time-lapse microscopy of constitutively PrD-GFP expressing strain carrying a Dot aggregate. Cells were monitored for several hours in the presence of 5 mM GdHCl to inhibit Hsp104 activity. Upon inhibition of Hsp104, cells with Dot aggregates gave rise to progeny forming Ring aggregates. Progeny thereof ultimately displayed diffuse fluorescence. Images show different representative groups of cells at different time points (0, 6, 24 h) and are an overlay of a single focal plane DIC image and a merge of fluorescence *z*-stack images.

A remaining question is how cells switch from the transitional Ring state to the mature prion state. One possibility is that a Ring-containing mother rarely but stochastically transmits a sufficiently large number of seeds to its daughter to create a profusion of shorter fibrils. Indeed, the number of wild-type [PSI^+] propagons is known to be clonally diverse (5). However, Ring and Dot cells contain the same quantity of the fibril fragmenting protein Hsp104 (Fig. S8), which plays a critical role in [PSI^+] inheritance (6, 29, 33–35). With just a few initiating fibrils, one might expect them to be highly susceptible to Hsp104, but Hsp104's remodeling functions are tightly regulated in unstressed cells (36). Thus, another explanation is a heritable switch in the activity of Hsp104. Speculatively, an inhibitor of Hsp104 might itself be a prion—the concentration of aggregated proteins at the IPOD could favor its switch to a heritable, nonfunctional state, converting Rings to highly fragmented mature prions.

However that specific detail may be resolved, many lines of evidence suggest that normal [PSI^+] induction, as well as the induction of other prions, involves a transitional state like the one we describe. For example, propagons of wild-type [PSI^+] are subject to biased retention in mother cells by a previously unknown mechanism (5). Both Rings and Dots are observed in cells with wild-type Sup35 during "typical" laboratory prion inductions with overexpressed PrD (11, 12), and Rings behave as an immature transitional state with unstable inheritance. Furthermore, in those cases where it has been examined, the induction of [PSI^+], [*URE3*], and [RNQ^+] by overexpression of their PrDs clearly involves a genetically unstable intermediate. Cells initially segregate both [$prion^-$] and [$PRION^+$] clones and only later stabilize to reliably produce [$PRION^+$] colonies (16–18, 37, 38). Finally, in the absence of PrD overexpression, proteotoxic stresses, including oxidative stresses, increase the spontaneous induction of [PSI^+] (9, 39). The more severe the stress, the more efficient the induction. Colocalization of damaged proteins at the IPOD could provide an opportunity for cross-seeding akin to that provided by [RNQ^+]. Subsequently, in the absence of PrD overexpression, the fragmentation activity of Hsp104 would be sufficient to free most of the assembled protein from the IPOD, allowing direct cytoplasmic inheritance of prion propagons.

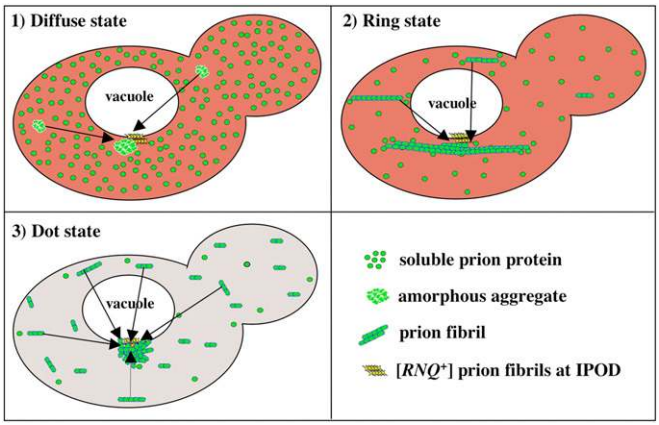

Fig. 6. Schematic model for the induction and maturation of the PrD-GFP prion via a long-lived poorly fragmented fibril state.

The concerted asymmetric retention of prion fibrils is tied to an ancient (but only recently discovered) system for the asymmetric inheritance of misfolded damaged proteins. Mitotic cells, ranging from bacteria to yeast to human embryonic stem cells, systematically retain and sequester damaged and misfolded proteins to one cell during division (26, 40, 41). This is thought to ensure the fitness of the next generation by allowing one of the two mitotic products to start afresh with respect to protein damage—segregating an aging (soma-like) lineage from a rejuvenated (germ-like) lineage. We propose that the IPOD is not only a depository for damaged proteins, but plays a critical positive role in prion biology as the cellular site of de novo prion induction.

Materials and Methods

Yeast Strains, Media, and Constructs. Yeast strains BY4741 (Euroscarf) and 74D-694 (6) were grown on standard synthetic media lacking particular amino acids/bases and containing either D-glucose (SD) or D-galactose (SGal) as carbon source. Sporulation was performed on 1% potassium acetate, 0.05% dextrose, 0.1% yeast extract, and 0.01% complete amino acid mix (BIO 101). Expression of PrD-GFP (9) was controlled by either the Gal1 or GPD promoter. The expression plasmid for RNQ1-CFP is described in ref. 15. Gene deletions used primer sequences listed at the yeast deletion project web site (www-sequence.stanford.edu/group/yeast_deletion_project/Deletion_primers_PCR_sizes.txt). Genomic C-terminal Cerulean fusions were confirmed by PCR. Plasmids coding for N-terminal Cerulean ATG8 or ATG14 fusions were generated using Gateway shuttle vectors (42) and the ORFs from the Open Biosystems mORF collection.

Seeding and Transformation. The seeding efficiency of crude lysates from cells with diffuse fluorescence, Rings, or Dots was tested with purified His-tagged protein using SDD-AGE as described in ref. 43. The same lysates were tested for transformation activity with a 74D-694-derived strain containing an *ADE1* mutation suppressible by [PSI^+] and a *URA3* plasmid as described in ref. 20. Details are provided in *SI Materials and Methods*.

Microscopy. Cells were grown in liquid culture to midlog phase or on agar plates overnight and examined with an Axioplan microscope with a ×100

CELL BIOLOGY

objective (Zeiss) and narrow band-pass filters for colocalization studies with different fluorescent proteins. Monoclonal HA antibody (Cell Signaling) and a secondary anti-mouse IgG antibody were coupled to Alexa Fluor 594 (Invitrogen). Unless indicated, images were taken in one representative focal plane. Photoshop was used for colorization, linear adjustments of brightness and contrast, and creation of composite and merged images. Time-lapse microscopy was performed on agarose pads of ~20 × 20 × 1 mm, prepared by pouring ultrapure agarose (2% wt/vol) in SD media directly onto a microscope slide. After addition of the cells, the pad was covered with a cover slide and sealed with melted VLAP wax (1:1:1 Vaseline:lanolin:paraffin). Every 60–90 min, we collected a stack of 12–15 optical sections spaced 0.4 μm apart. Representative fluorescence images were de-blurred using a simple deconvolution algorithm and then projected to one image. For conventional and immunoelectron microscopy details, see *SI Materials and Methods*.

ACKNOWLEDGMENTS. We thank K. Allendoerfer, K. K. Frederick, R. Krishnan, and S. Alberti for critical reading of the manuscript; E. Spooner (Whitehead Institute) for mass spectrometry; and M. J. Sa and A. W. Murray (Harvard University) for assistance with time-lapse microscopy. This work was supported by National Institutes of Health Grant GM025874 (to S.L.), a European Molecular Biology Organization Long-Term Fellowship (to J. T.), a Human Frontiers Science Program Organization Long-Term Fellowship (to J.T.), and an American Heart Association fellowship (to J.D.). S.L. is an Investigator of the Howard Hughes Medical Institute.

1. Shorter J, Lindquist S (2005) Prions as adaptive conduits of memory and inheritance. *Nat Rev Genet* 6:435–450.
2. Chernoff YO (2007) Stress and prions: lessons from the yeast model. *FEBS Lett* 581: 3695–3701.
3. Halfmann R, Alberti S, Lindquist S (2010) Prions, protein homeostasis, and phenotypic diversity. *Trends Cell Biol* 20:125–133.
4. Alberti S, Halfmann R, King O, Kapila A, Lindquist S (2009) A systematic survey identifies prions and illuminates sequence features of prionogenic proteins. *Cell* 137: 146–158.
5. Cox B, Ness F, Tuite M (2003) Analysis of the generation and segregation of propagons: entities that propagate the [PSI+] prion in yeast. *Genetics* 165:23–33.
6. Chernoff YO, Lindquist SL, Ono B, Inge-Vechtomov SG, Liebman SW (1995) Role of the chaperone protein Hsp104 in propagation of the yeast prion-like factor [psi+]. *Science* 268:880–884.
7. Glover JR, et al. (1997) Self-seeded fibers formed by Sup35, the protein determinant of [PSI+], a heritable prion-like factor of S. cerevisiae. *Cell* 89:811–819.
8. True HL, Lindquist SL (2000) A yeast prion provides a mechanism for genetic variation and phenotypic diversity. *Nature* 407:477–483.
9. Tyedmers J, Madariaga ML, Lindquist S (2008) Prion switching in response to environmental stress. *PLoS Biol* 6:2605–2613.
10. Chernoff YO, Derkach IL, Inge-Vechtomov SG (1993) Multicopy SUP35 gene induces de-novo appearance of psi-like factors in the yeast Saccharomyces cerevisiae. *Curr Genet* 24:268–270.
11. Zhou P, Derkatch IL, Liebman SW (2001) The relationship between visible intracellular aggregates that appear after overexpression of Sup35 and the yeast prion-like elements [PSI(+)] and [PIN(+)]. *Mol Microbiol* 39:37–46.
12. Ganusova EE, et al. (2006) Modulation of prion formation, aggregation, and toxicity by the actin cytoskeleton in yeast. *Mol Cell Biol* 26:617–629.
13. Patino MM, Liu JJ, Glover JR, Lindquist S (1996) Support for the prion hypothesis for inheritance of a phenotypic trait in yeast. *Science* 273:622–626.
14. Vishveshwara N, Bradley ME, Liebman SW (2009) Sequestration of essential proteins causes prion associated toxicity in yeast. *Mol Microbiol* 73:1101–1114.
15. Sondheimer N, Lindquist S (2000) Rnq1: an epigenetic modifier of protein function in yeast. *Mol Cell* 5:163–172.
16. Derkatch IL, Bradley ME, Hong JY, Liebman SW (2001) Prions affect the appearance of other prions: the story of [PIN(+)]. *Cell* 106:171–182.
17. Osherovich LZ, Weissman JS (2001) Multiple Gln/Asn-rich prion domains confer susceptibility to induction of the yeast [PSI(+)] prion. *Cell* 106:183–194.
18. Derkatch IL, et al. (2000) Dependence and independence of [PSI(+)] and [PIN(+)]: a two-prion system in yeast? *EMBO J* 19:1942–1952.
19. King CY, Diaz-Avalos R (2004) Protein-only transmission of three yeast prion strains. *Nature* 428:319–323.
20. Tanaka M, Chien P, Naber N, Cooke R, Weissman JS (2004) Conformational variations in an infectious protein determine prion strain differences. *Nature* 428:323–328.
21. Tanaka M, Collins SR, Toyama BH, Weissman JS (2006) The physical basis of how prion conformations determine strain phenotypes. *Nature* 442:585–589.
22. Zhou P, et al. (1999) The yeast non-Mendelian factor [ETA+] is a variant of [PSI+], a prion-like form of release factor eRF3. *EMBO J* 18:1182–1191.
23. He C, Klionsky DJ (2009) Regulation mechanisms and signaling pathways of autophagy. *Annu Rev Genet* 43:67–93.
24. Kaganovich D, Kopito R, Frydman J (2008) Misfolded proteins partition between two distinct quality control compartments. *Nature* 454:1088–1095.
25. Cabiscol E, Piulats E, Echave P, Herrero E, Ros J (2000) Oxidative stress promotes specific protein damage in Saccharomyces cerevisiae. *J Biol Chem* 275:27393–27398.
26. Aguilaniu H, Gustafsson L, Rigoulet M, Nyström T (2003) Asymmetric inheritance of oxidatively damaged proteins during cytokinesis. *Science* 299:1751–1753.
27. Liu B, et al. (2010) The polarisome is required for segregation and retrograde transport of protein aggregates. *Cell* 140:257–267.
28. Krzewska J, Melki R (2006) Molecular chaperones and the assembly of the prion Sup35p, an in vitro study. *EMBO J* 25:822–833.
29. Ness F, Ferreira P, Cox BS, Tuite MF (2002) Guanidine hydrochloride inhibits the generation of prion "seeds" but not prion protein aggregation in yeast. *Mol Cell Biol* 22:5593–5605.
30. Kawai-Noma S, et al. (2006) Dynamics of yeast prion aggregates in single living cells. *Genes Cells* 11:1085–1096.
31. Serio TR, et al. (2000) Nucleated conformational conversion and the replication of conformational information by a prion determinant. *Science* 289:1317–1321.
32. Derkatch IL, et al. (2004) Effects of Q/N-rich, polyQ, and non-polyQ amyloids on the de novo formation of the [PSI+] prion in yeast and aggregation of Sup35 in vitro. *Proc Natl Acad Sci USA* 101:12934–12939.
33. Borchsenius AS, Müller S, Newnam GP, Inge-Vechtomov SG, Chernoff YO (2006) Prion variant maintained only at high levels of the Hsp104 disaggregase. *Curr Genet* 49: 21–29.
34. Borchsenius AS, Wegrzyn RD, Newnam GP, Inge-Vechtomov SG, Chernoff YO (2001) Yeast prion protein derivative defective in aggregate shearing and production of new 'seeds'. *EMBO J* 20:6683–6691.
35. Wegrzyn RD, Bapat K, Newnam GP, Zink AD, Chernoff YO (2001) Mechanism of prion loss after Hsp104 inactivation in yeast. *Mol Cell Biol* 21:4656–4669.
36. Schirmer EC, Homann OR, Kowal AS, Lindquist S (2004) Dominant gain-of-function mutations in Hsp104p reveal crucial roles for the middle region. *Mol Biol Cell* 15: 2061–2072.
37. Fernandez-Bellot E, Guillemet E, Cullin C (2000) The yeast prion [URE3] can be greatly induced by a functional mutated URE2 allele. *EMBO J* 19:3215–3222.
38. Salnikova AB, Kryndushkin DS, Smirnov VN, Kushnirov VV, Ter-Avanesyan MD (2005) Nonsense suppression in yeast cells overproducing Sup35 (eRF3) is caused by its non-heritable amyloids. *J Biol Chem* 280:8808–8812.
39. Sideri TC, Stojanovski K, Tuite MF, Grant CM (2010) Ribosome-associated peroxiredoxins suppress oxidative stress-induced de novo formation of the [PSI +] prion in yeast. *Proc Natl Acad Sci USA*, 10.1073/pnas.1000347107.
40. Lindner AB, Madden R, Demarez A, Stewart EJ, Taddei F (2008) Asymmetric segregation of protein aggregates is associated with cellular aging and rejuvenation. *Proc Natl Acad Sci USA* 105:3076–3081.
41. Rujano MA, et al. (2006) Polarised asymmetric inheritance of accumulated protein damage in higher eukaryotes. *PLoS Biol* 4:2325–2335.
42. Alberti S, Gitler AD, Lindquist S (2007) A suite of Gateway cloning vectors for high-throughput genetic analysis in Saccharomyces cerevisiae. *Yeast* 24:913–919.
43. Bagriantsev SN, Kushnirov VV, Liebman SW (2006) Analysis of amyloid aggregates using agarose gel electrophoresis. *Methods Enzymol* 412:33–48.

Supporting Information

Tyedmers et al. 10.1073/pnas.1003895107

SI Materials and Methods

Electron Microscopy. Conventional and immunoelectron microscopy were performed as described in ref. 1, but with some changes, as described below.

For conventional EM, yeast cells were harvested by centrifugation and resuspended in fix [3% glutaraldehyde, 0.1 M sodium cacodylate, 5 mM $CaCl_2$ (pH 6.8)]. Cells were fixed for 1 h at room temperature, washed, and resuspended in 1.2 M sorbitol in phos-citrate buffer (0.1 M K_2HPO_4, 0.033 M citric acid). The fixed cells were then treated with glucuronidase and zymolyase for 1 h to remove the cell walls, as described in ref. 2. Cells were embedded in 2% ultra-low gelling temperature (Sigma, type IX), stained with osmium/thiocarbohydrazide as described in ref. 3, and embedded in low-viscosity Spurr plastic resin for 48 h at 60 °C. Sections (80 nm) were cut on a Leica UCT ultramicrotome, stained with lead citrate and uranyl acetate, respectively, and examined at 80 kV using a Philips EM 410 transmission electron microscope. Images were collected with a Soft Imaging System Megaview III camera, and figures were assembled in Adobe Photoshop with only linear adjustments in brightness and contrast.

For Immuno-EM, cells were fixed in suspension for 15 min by adding an equal volume of freshly prepared 8% formaldehyde contained in 100 mM PO_4 buffer (pH 7.4). The cells were pelleted, resuspended in fresh fixative [4% formaldehyde/100 mM PO_4 (pH 7.4)], and incubated for an extra 18–24 h at 4 °C. The cells were washed briefly in PBS and resuspended in 2% low-gelling-temperature agarose. The agarose blocks were trimmed into pieces of 1 mm^3, cryoprotected by infiltration with 2.3 M sucrose/20% polyvinyl pyrrolidone (10,000)/PBS (pH 7.4) for 2 h, mounted on cryopins, and rapidly frozen in liquid nitrogen. Ultrathin cryosections were cut on a Leica UCT ultramicrotome equipped with an FC-S cryoattachment and collected onto formvar/carbon-coated nickel grids. The grids were washed through several drops of PBS containing 2.5% FCS and 10 mM glycine (pH 7.4) and then blocked in 10% FCS for 30 min and incubated overnight in 10 mg/mL chicken anti-GFP antibody (Abcam) and a 1:200 dilution of rabbit anti-α-1,6 mannose serum. After washing, the grids were incubated for 2 h in 12 nm Au donkey anti-rabbit conjugate or 6 nm Au donkey anti-chicken (Jackson ImmunoResearch). The grids were washed through several drops of PBS followed by several drops of ddH_2O. Grids were then embedded in an aqueous solution containing 3.2% polyvinyl alcohol (10,000), 0.2% methyl cellulose (400 centiposes), and 0.1% uranyl acetate.

Immunofluorescence. This method was performed in general as described in ref. 3 with some modifications. The detailed method used is given below.

Fixation and spheroblasting. An overnight culture was grown in selective media to saturation and used to inoculate a fresh culture. Eight milliliters of cells was harvested at an OD_{600} of 0.6 and placed onto a bottle top filter (0.2-μm pores). After the liquid was removed by vacuum, cells were immediately resuspended in 5 mL of 4% formaldehyde in 50 mM KPO_4 (pH 6.5)/1 mM $MgCl_2$ and incubated for 2 h at room temperature in a 15-mL screw cap tube. Cells were collected by centrifugation for 3 min at 1,000 × *g*, washed in 50 mM KPO_4 (pH 6.5)/1 mM $MgCl_2$ containing a protease inhibitor mixture (Roche 1 836 170), and resuspended in the same buffer to an OD_{600} of 10. Seven microliters of a 1 mg/mL zymolyase T100 solution and 0.6 μL of 2-mercaptoethanol were added to 100 μl of cells and incubated for 30 min at 30 °C. Spheroblasts were washed by centrifugation for 2 min at 1,000 × *g* and resuspended carefully in 100 μL of 50 mM KPO_4 (pH 6.5)/1 mM $MgCl_2$ containing a protease inhibitor mixture (Roche 1 836 170).

Adhesion of cells to microscope slide. Wells on a cover slide were created using an adhesive courier document pouch and a rotating-head hole puncher, coated with 0.1% polylysine (Sigma #P-1524) and washed three times with water before 10 μL of spheroblasts per well was added. After 3 min of adhesion, excess liquid was removed and the coverslip was dried completely before it was immersed in precooled (−20 °C) acetone for 5 min. After blotting away excess solvent, the coverslip was dried before blocking and antibody incubation steps followed.

Antibody incubation. For blocking, each well was incubated with a drop of PBS-block (1% milk powder, 0.1% BSA, 0.1% octyl glucoside) for 30 min before the primary antibody [monoclonal mouse anti-HA-tag antibody (6E2) from cell signaling, lot 1B # 2367] in PBS-block was added and incubated for 60 min at room temperature in a humid chamber. Each well was washed eight times with PBS-block before the secondary antibody (Alexa Fluor 594 anti-mouse IgG A11062, lot #57764a from Invitrogen) was added and incubated for 30 min in the dark. Subsequently, cells were washed eight times, excess liquid was removed, and 5 μL of mounting media per well was added before the coverslip was inverted onto a slide and sealed with nail polish.

Cell Lysis of Strains Displaying Diffuse, Ring- or Dot-Shaped Aggregates for PrD-Seeding Reactions and Protein Transformations. Strains carrying PrD-GFP under control of a Gal-inducible promoter and displaying diffuse, Ring- or Dot-shaped aggregation patterns of PrD-GFP were grown in SGal media to an OD of between 1 and 2. For the Ring cultures, this yielded the largest fraction of cells displaying Ring aggregates (~70%). Harvested cell pellets were frozen before resuspension in chilled lysis buffer [50 mM Tris·HCl (pH 7.4), 200 mM NaCl, 2 mM TCEP, 5% glycerol, 1 mM EDTA, 4 mM PMSF, 5 μg/mL aprotinin, 5 μg/mL leupeptin, 1 tablet of complete protease inhibitor mixture (Roche)]. An equal volume of glass beads was added to the pellet suspension and crude lysates were generated by bead beating for 10 min on a Qiagen tissue-lyser. Crude lysates were precleared at 500 rcf for 2 min at 4 °C. The total amount of PrD-GFP in different lysates was assessed by immunoblotting with a GFP antibody.

Protein Transformation. Yeast cells with an *ADE1* mutation suppressible by [PSI^+] (*MAT*α *leu2-3, -112 his3-11 trp1-1 ura3-1 ade1-14 can1-100* [*pin-*] [*psi-*] [*ure-o*]) were cotransformed with PrD-GFP from crude lysates of cells with diffuse, Ring or Dot fluorescence and a *URA3* plasmid as described in ref. 4 and summarized here. Yeast cells were grown in 50 mL of YPD at 30 °C to OD_{600} ~0.5–0.6. Cells were recovered by centrifugation at 3,000 × *g* for 5 min at 25 °C and washed once with sterile distilled water, once with 1 M sorbitol, and then with SCE buffer [1 M sorbitol, 10 mM EDTA, 10 mM DTT, 100 mM sodium citrate (pH 5.8)]. After resuspension in 1mL of SCE buffer, cells were incubated with lyticase (200 units/mL) for 30 min at 30 °C. Spheroblasts were recovered and washed with 1 M sorbitol followed by STC buffer [1 M sorbitol, 10 mM $CaCl_2$, 10 mM Tris·HCl (pH 7.5)] and finally resuspended in 1 mL of STC buffer. Twenty-five microliters of crude lysates (2 mg/mL total protein concentration) of yeast cells displaying diffuse, Ring or Dot fluorescence of PrD-GFP was mixed with a *URA3* plasmid and salmon sperm DNA. Spheroblasts were added to the protein solution and incubated for 30 min at 25 °C. Fusion of spheroblasts

with plasmid/protein complexes was induced by addition of 9 vol of PEG-buffer [20% PEG 8000, 10 mM $CaCl_2$, 10 mM Tris·HCl (pH 7.5)] and incubation for 30 min at 25 °C. Spheroblasts were recovered and resuspended in SOS buffer (1 M sorbitol, 0.25% yeast extract, 0.5% bacto-peptone, 7 mM $CaCl_2$) and incubated for 30 min at 30 °C. Recovered transformants were mixed with 7 mL of URA dropout top agar (2.5% agar at 45 °C containing 1 M sorbitol) and immediately poured onto URA dropout plates (containing 1 M sorbitol). After incubation at 30 °C for 4–5 days, ≈100 Ura^+ colonies were randomly chosen and streaked onto modified YEPD plates containing 1/4 of the standard amount of yeast extract to enhance color phenotypes of [PSI^+] and [psi^-] states.

Seeding Efficiency of Cell Lysates Displaying Different PrD-GFP Aggregation Patterns. Equilibrated crude lysates from cells displaying diffuse, Ring or Dot fluorescence of PrD-GFP were added to reaction tubes containing 5 μM of purified His-tagged PrD in 1× CRBB buffer [5 mM potassium phosphate (pH 7.4), 150 mM NaCl, 5 μg/mL aprotinin, 5 μg/mL leupeptin]. The reactions were incubated at room temperature without agitation. Polymerization time points were harvest by adding 2% SDS sample buffer [2× TAE, 20% glycerol, 8% SDS (wt/vol), bromophenol blue] and snap-freezing them. Formation of SDS-resistant aggregates was assessed by SDD-AGE and probing with a His antibody (5, 6).

Immunoprecipitation. Cells expressing PrD-GFP under control of the GPD-promoter displaying diffuse PrD-GFP fluorescence ([prd-gfp−]) or Dots ([PrD-GFP+]) were grown in selective media to an OD of ~0,6, harvested, washed with water, resuspended in spheroblasting buffer [1 M sorbitol, 0.1 M EDTA, 0.5 mg/mL zymolyase T-100 (Seikagaku), 20 mM DTT], and incubated for 30 min at 30 °C to remove the cell wall. After pelleting the spheroblasts, they were resuspended in IP buffer [50 mM Hepes (pH 7.5), 150 mM NaCl, 2.5 mM EDTA, 1% Triton X-100, 40 mM NEM, 1 mM PMSF, 1 Roche inhibitor mix tablet/5 mL]. Glass beads were added and beat in a bead beater for 2 min at 4 °C. Lysates were incubated with an anti-GFP antibody and incubated for 1.5 h at 4 °C. Subsequently, BSA-blocked Dynal beads were added to the lysates and further incubated for 4 h at 4 °C. After rigorous washing with IP buffer, proteins bound to the beads were eluted with Laemmli sample buffer [50 mM Tris·HCl (pH 6.8), 2% BME, 2% SDS, 10% glycerol] followed by SDS/PAGE and Coomassie brilliant blue staining.

Mass Spectrometry. Proteins present in bands that were cut out of the gel, fragmented by trypsin digest, and separated by HPLC (Waters nanoACQUITY) using a 0.075-μm-diameter column with a flow rat of 250 nl/min. The eluant from this was introduced into a linear ion-trap tandem mass spectrometer (Thermo LTQ) equipped with a nanospray source. The resulting CID spectra were searched against a protein database using SEQUEST.

1. Rieder SE, Banta LM, Köhrer K, McCaffery JM, Emr SD (1996) Multilamellar endosome-like compartment accumulates in the yeast vps28 vacuolar protein sorting mutant. *Mol Biol Cell* 7:985–999.
2. Banta LM, Robinson JS, Klionsky DJ, Emr SD (1988) Organelle assembly in yeast: characterization of yeast mutants defective in vacuolar biogenesis and protein sorting. *J Cell Biol* 107:1369–1383.
3. Rossanese OW, et al. (1999) Golgi structure correlates with transitional endoplasmic reticulum organization in Pichia pastoris and Saccharomyces cerevisiae. *J Cell Biol* 145: 69–81.
4. Tanaka M, Weissman JS (2006) An efficient protein transformation protocol for introducing prions into yeast. *Methods Enzymol* 412:185–200.
5. Bagriantsev SN, Kushnirov VV, Liebman SW (2006) Analysis of amyloid aggregates using agarose gel electrophoresis. *Methods Enzymol* 412:33–48.
6. Halfmann R, Lindquist S (July 16, 2008) Screening for amyloid aggregation by semi-denaturing detergent-agarose gel electrophoresis. *J Vis Exp*, 17, 10.3791/838.

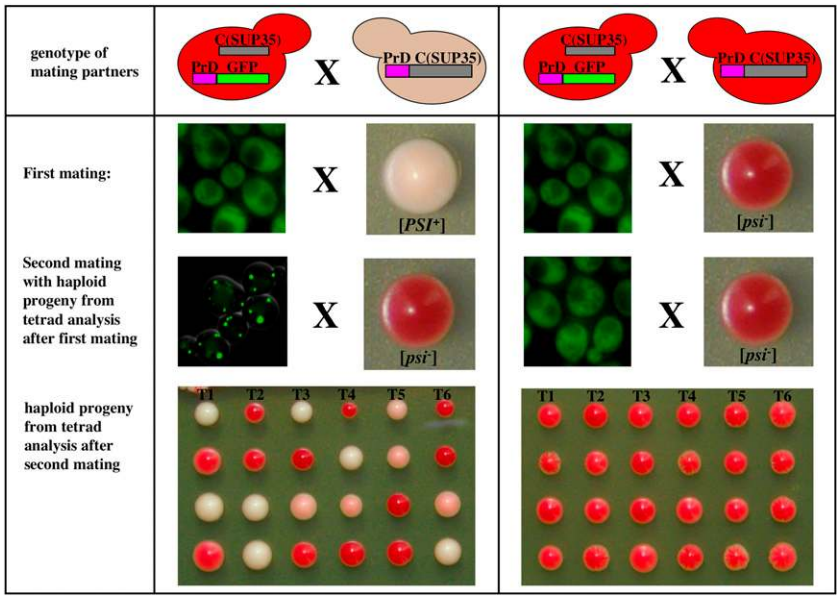

Fig. S1. PrD-GFP is a prion on its own right. To reveal whether PrD-GFP can act as an independent prion, haploid strains with a deletion of PrD in the endogenous SUP35 gene (C(SUP35)) that expressed PrD-GFP under control of the Sup35 promoter (concentrations comparable to wild-type Sup35 (PrD-C(SUP35)) and displayed diffuse GFP fluorescence were used. A first mating involved a mating partner with wild-type Sup35 in [*PSI*$^+$] to induce the prion conformation in PrD-GFP (left panel). A similar mating with a [*psi*$^-$] strain served as a control (right panel). Haploid progeny from the first mating that contained the PrD-GFP fusion and the C(SUP35) allele was analyzed by fluorescence microscopy and revealed that only mating of PrD-GFP with a [*PSI*$^+$] strain resulted in formation of PrD-GFP aggregates (left panel, middle). Subsequently, this progeny was mated to a [*psi*$^-$] strain wild type for SUP35 and revealed that PrD-GFP in its aggregated state could transmit the prion state to the wild-type SUP35 protein in a mating partner (bottom, left panel).

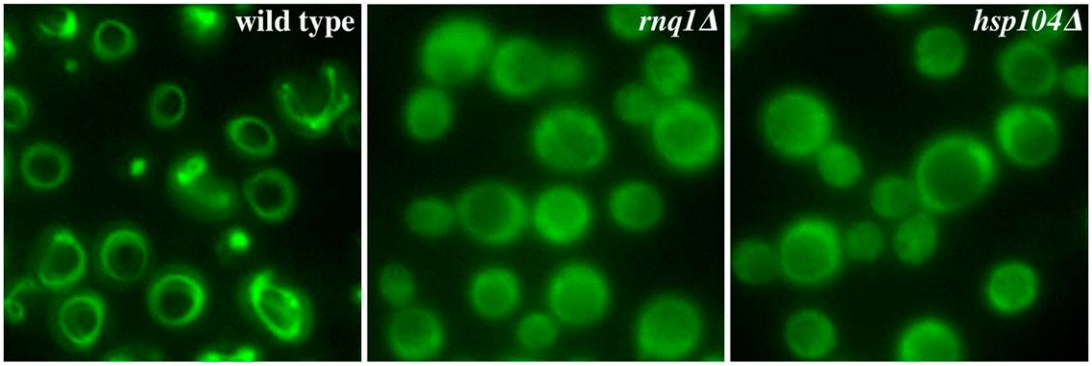

Fig. S2. The formation of Ring aggregates and Dot aggregates requires HSP104 and RNQ1. Constitutive expression PrD-GFP under control of the GPD promoter (compare with Fig. *A*) results in Ring- and Dot aggregates in a control strain (wild type), but only diffuse fluorescence or in a strain with the deletion of RNQ1 (*rnq1*Δ) or HSP104 (*hsp104*Δ).

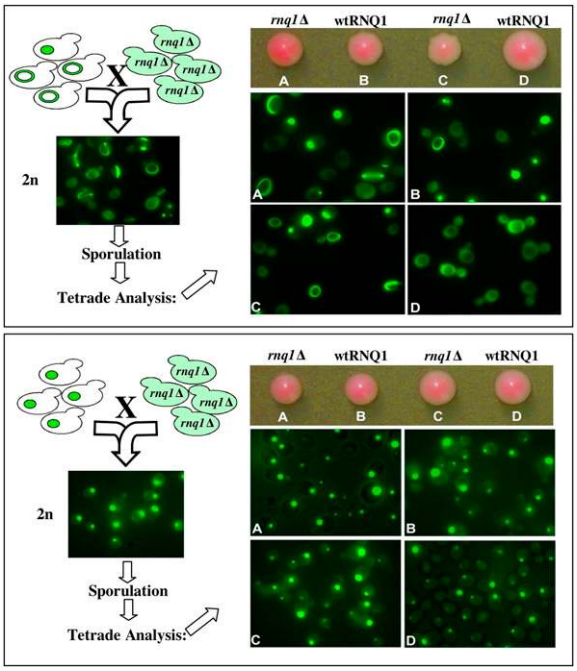

Fig. S3. Both Ring and Dot aggregates can propagate in the absence of Rnq1. Haploid strains carrying a PrD deletion in the endogenous SUP35 gene that expressed PrD-GFP under control of the GPD promoter and displayed mostly Rings (*A*) or only Dots (*B*) were mated to an equivalent strain that carried additionally a deletion of RNQ1 and displayed diffuse PrD-GFP fluorescence (compare with Fig. S2). The resulting diploids were analyzed by fluorescence microscopy and displayed mostly Ring-aggregates (A, left) or only Dots (B, left). After sporulation and tetrad analysis, spores were genotyped by PCR to detect segregation of wild-type RNQ1 (wtRNQ1) and the corresponding deletion (*rnq1*Δ) and analyzed for PrD-GFP-fluorescence. Rings and Dots both propagated also in the absence of RNQ1.

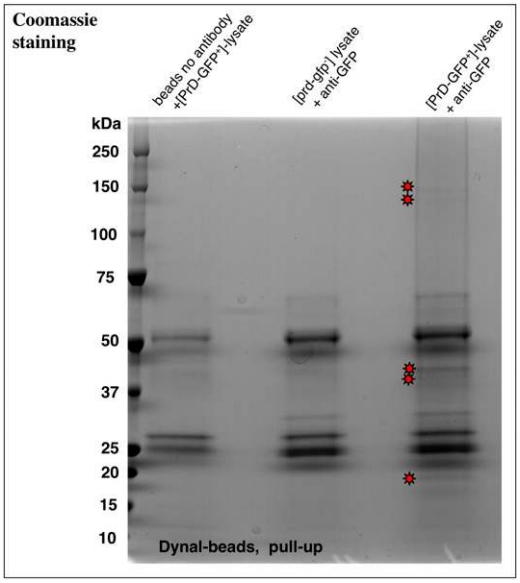

Fig. S4. Co-purification of proteins with PrD-GFP from cell lysates with Dot aggregates. (*A*) Coomassie stain of eluate fractions from immuno-precipitations with lysates from cells expressing PrD-GFP and displaying Dots ([PrD-GFP$^+$]-lysates) or diffuse fluorescence ([prd-gfp$^-$]-lysate) were incubated with no antibody (control, left lane) or antibodies against GFP (middle and right lanes). Magnetic Dynal beads coated with protein A were used to isolate antibody–protein complexes from the lysates. Stars indicate protein bands occurring specifically when lysates from cells with PrD-GFP in Dot aggregates were used. Size ranges of ~10 kDa steps were cut out of the gel from eluates of cells with diffuse fluorescence (control) and Dot fluorescence and analyzed by mass spectrometry. (*B*) Table of proteins present only in protein bands isolated from Dot cell lysates but not cell lysates with diffuse PrD-GFP fluorescence. At least two different peptides of each listed protein were identified by mass spectrometry.

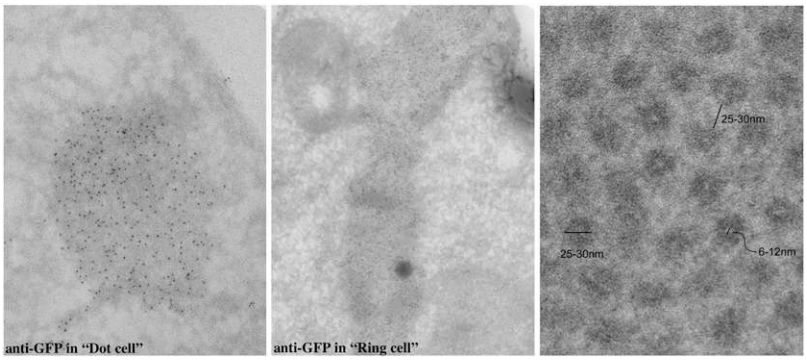

Fig. S5. Characterization of PrD-GFP in Ring- or Dot aggregates by immuno-EM and determination of the dimensions in PrD-GFP fibrils. (*A*) Ultrathin sections of a cell with Dots (left) or Rings (right) were analyzed by immuno-EM with an antibody against GFP labeled with immunogold and confirmed that PrD-GFP is present in areas with accumulated fibrils. (*B*) Magnification of perpendicular section of a Ring aggregate allows measuring the diameter of the inner core of the fibril (6–12 nm), the entire fibril (25–30 nm), and the spacing between two fibrils (25–30 nm). Identical measures were found for bundles of fibrils from Dot aggregates.

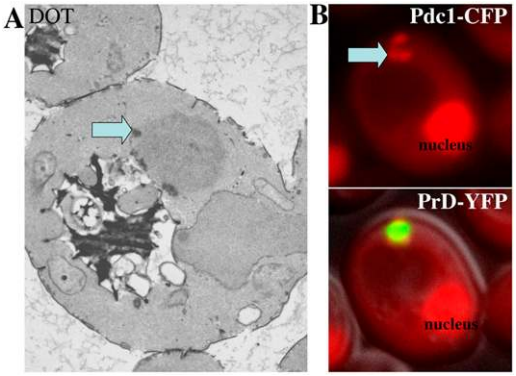

Fig. S6. Prion fibril accumulations at the IPOD are partially surrounded by electron-dense material typical for amorphously aggregated proteins. A different cutout of the same DOT-cell as shown in the electron micrograph in Fig. 5*A Lower Left* is compared with a magnification of Fig. 4*B*, right column. The latter displays a fluorescence microscopy image of cells expressing PrD-YFP and Pdc1-CFP after incubation with low concentrations of menadione (0.1 mM) for 4 h.

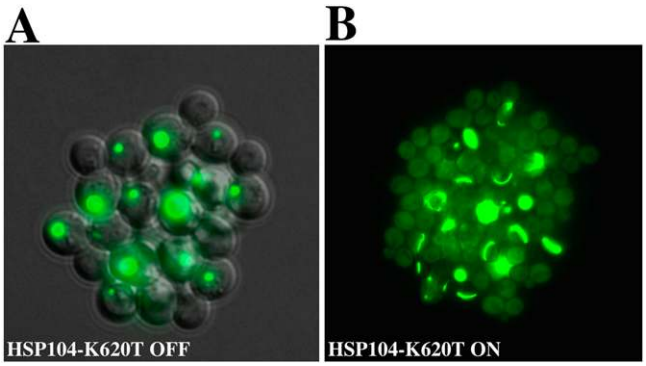

Fig. S7. Expression of the dominant negative HSP104 mutant K620T induces the formation of PrD-GFP Rings in the progeny of Dot-containing cells. A haploid strain with a deletion of PrD in the endogenous SUP35 gene that expressed PrD-GFP under control of the GPD promoter and propagated the Dot state was transformed with a plasmid coding for the dominant negative HSP104 mutant HSP104-K620T [Parsell DA, Sanchez Y, Stitzel JD, Lindquist S (1991) *Nature* 353:270–273] under control of a glucocorticoid inducible promoter [Schirmer EC, Lindquist S (1998) *Methods Enzymol* 290:430–444]. Cells were placed on an agarose pad on a microscope slide either lacking (*A*) or containing (*B*) 10 μM deoxycorticosterone to induce expression of the HSP104 mutant and allowed to divide for several hours. The images represent a merge of several focal planes taken at the end (12 h) of time-lapse microscopy experiments.

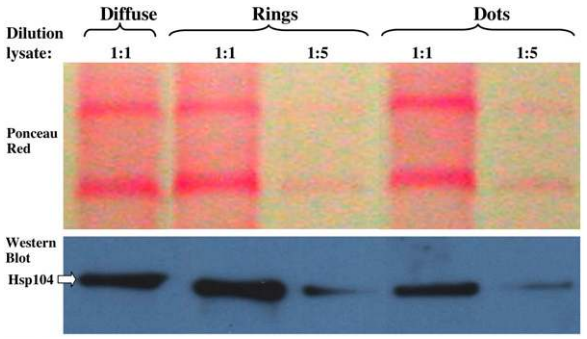

Fig. S8. Similar levels of Hsp104 in cells with diffuse PrD-GFP fluorescence, PrD-GFP Rings or Dots. Different dilutions of cell lysates from cells displaying diffuse, Ring or Dot fluorescence were subjected to SDS/PAGE followed by Western blot analysis onto PVDF membranes. The PVDF membranes were stained with Ponceau-S (*Upper*) to control for loading and subsequently incubated with an antibody against Hsp104 (*Lower*).

Table S1. Proteins copurifying specifically with PrD-GFP Dots

METABOLIC ENZYMES AND RIBOSOMAL PROTEINS Rpl30, Rps9bp, Rpl21ap, Rpl11, Rpl4a, Rpl5	
Ade1p	Phosphoribosyl amino imidazole succinocarbozamide synthetase
Rhr2	DL-glycerol-3-phosphatase
Adh1	Alcohol dehydrogenase
Oye2	NAPDH dehydrogenase (old yellow enzyme), isoform 2
Sam2	*S*-adenosylmethionine synthetase
Eno1	Enolase I
Eno2	Enolase II
Glc7	Lactoylglutathione lyase (glyoxalase I)
Glo1	Lactoylglutathione lyase (glyoxalase I)
Sah1	Putative *S*-adenosyl-L-homocysteine hydrolase
Cdc19	Pyruvate kinase
Pdc1	Pyruvate decarboxylase
Ded81	Asparaginyl-tRNA synthetase
Tkl1	Transketolase 1
Ade3	Cytoplasmic trifunctional enzyme C1-tetrahydrofolate synthase
CHAPERONES	
Sis1	Type II HSP40 co-chaperone that interacts with the HSP70 protein Ssa1p
Ydj1	Protein chaperone; member of the DnaJ family
Cph1	Cytoplasmic peptidyl-prolyl cis-trans isomerase
CYTOSKELETON	
Nap1	Regulation of microtubule dynamics during mitosis; controls bud morphogenesis
Bni1	Formin, nucleates the formation of linear actin filaments
Arc19	Subunit of the ARP2/3 complex, motility and integrity of cortical actin patches
PROTEASOME	
Pre3	20S proteasome β-type subunit,
Pre1	20S proteasome β-type subunit
OTHER	
Rnq1	[PIN(+)] prion
Ypt1	Ras-like small GTPase, involved in the ER-to-Golgi step of the secretory pathway
Sgn1	Cytoplasmic RNA-binding protein; may have a role in mRNA translation